





Model dielectric functions for fluctuation potential calculations in electron gas: A critical assessment

Aditi Mandal ^{1,2}, Sylvain Tricot ², Rakesh Choubisa ¹, and Didier Sébilleau ^{2,*}

¹Department of Physics, Birla Institute of Technology and Science–Pilani, Pilani Campus, Pilani, Rajasthan 333031, India

²Université de Rennes, CNRS, IPR (Institut de Physique de Rennes) - UMR 6251, F-35000 Rennes, France



(Received 21 January 2022; revised 29 March 2022; accepted 1 April 2022; published 19 May 2022)

In this article, we report on a critical assessment of dielectric function calculations in electron gas through the comparison of different modeling methods. This work is motivated by the fact that the dielectric function is a key quantity in the multiple scattering description of plasmon features in various electron-based spectroscopies. Starting from the standard random phase approximation (RPA) expression, we move on to correlation-augmented RPA, then damped RPA models. Finally, we study the reconstruction of the dielectric function from its moments, using the Nevanlinna and memory function approaches. We find the memory function method to be the most effective, being highly flexible and customizable.

DOI: [10.1103/PhysRevB.105.195424](https://doi.org/10.1103/PhysRevB.105.195424)

I. INTRODUCTION

Plasmon effects occur in many electron-driven spectroscopies and are the signature of the response of the system to the sudden appearance of an extra charge (a traveling electron, a hole left behind, etc.). In core-level photoemission for instance, plasmons appear as separate peaks at energies below the core peak. The energy differences with the core peaks are multiples of the plasmon energy $n\hbar\omega_p$. Here, n is the number of plasmon losses suffered by the photoelectron before escaping the material under study. Values of n at least up to 6 have been observed by Barman and coworkers [1] in aluminum. More recent results using 6 keV hard x-ray photoelectron spectroscopy (HAXPES) seem to exhibit up to 14 plasmon peaks [2]. For surface-sensitive photoemission, the surface plasmon peak can be distinguished from the bulk one as they appear at different energies.

The information embedded into plasmon peaks has not been much studied so far in photoemission. Back in 1990, Osterwalder and coworkers showed that they exhibited photoelectron-diffraction-like features just as their core-level peak [3]. More recently, David, Godet, and coworkers proposed to use these plasmon peaks to extract from their energy distribution some information on the system's dielectric function [4,5]. They termed this new spectroscopy “photoemission electron energy loss spectroscopy” (PEELS). Similarly, plasmon structures originating from valence band electrons have also been studied by Guzzo and coworkers [6,7]. Therefore, although not used that much yet as a system's information provider, plasmon structures seem a promising tool to extract some new information from spectroscopies, and in our case, from photoemission.

From the theoretical point of view, Hedin and coworkers introduced two approaches in order to model plasmon features in photoemission and x-ray absorption: the GW + cumulant

expansion and the quasiboson model Hamiltonian method [6–8]. The two methods have been shown to be formally equivalent by Vigil-Fowler *et al.* [8]. The GW + cumulant expansion has been favored by Reining and coworkers [6,7] to model plasmon structures originating from valence bands. They showed in particular that neither DFT nor GW were able to model the plasmon satellite. On the other side, Fujikawa and coworkers have used Hedin's quasiboson model in order to incorporate it into the multiple scattering description of spectroscopies [9–11]. Following Fujikawa's approach, it can be shown that, using reasonable approximations, the first plasmon peak cross section can be written as the product of the core peak cross section times a loss function, which is very convenient as standard multiple scattering codes such as MsSpec [12,13] compute the core peak cross section. Therefore, the implementation of the plasmon peak into a core-level code only involves the computation of this loss function. Fujikawa and coworkers have shown that this function can be expressed as [11]

$$\int f_c(\mathbf{r})V^i(\mathbf{r})d\mathbf{r}, \quad (1)$$

where $f_c(\mathbf{r})$ is a function involving the core-hole wave function and the escaping photoelectron wave function. $V^i(\mathbf{r})$ is the so-called fluctuation potential that describes the excitation of a plasmon (by either the core hole or the photoelectron). The only unknown in this approach is the fluctuation potential. Both Hedin and Fujikawa have used for $V^i(\mathbf{r})$ the analytical expressions derived either by Inglesfield [14] or by Bechstedt [15,16]. These descriptions are based on a 3D metallic-type material with a well-identified surface, and for photoelectrons of low kinetic energies, originating from the vicinity of the surface. Therefore, they completely exclude lower-dimensional systems (quantum dots, quantum wires, quantum wells, etc.) or semiconductors, heterostructures, and Dirac systems such as graphene and related layers or bilayers. Moreover, they are not suited to HAXPES experiments where the surface is basically overlooked by the escaping electron.

*didier.sebilleau@univ-rennes1.fr

In order to treat more diverse types of materials and spectroscopies involving more energetic electrons, we propose an alternative method to the problem of the description of the fluctuation potential. For this, we go back to the definition that was given by Hedin and coworkers. In Ref. [15] they define this potential as

$$V^{\mathbf{q}}(\mathbf{r}) = \left| \frac{V_C(\mathbf{q})}{\frac{\partial \varepsilon(\mathbf{q}, \omega)}{\partial \omega} \Big|_{\omega=\omega(\mathbf{q})}} \right|^{1/2} e^{i\mathbf{q}\cdot\mathbf{r}}, \quad (2)$$

where $V_C(\mathbf{q})$ is the Fourier transform of the Coulomb potential and $\varepsilon(\mathbf{q}, \omega)$ is the dielectric function of the system. The derivation is taken along the plasmon dispersion $\omega(\mathbf{q})$ which can be obtained by solving $\text{Re}[\varepsilon(\mathbf{q}, \omega)] = 0$, where $\text{Re}[\dots]$ indicates the real part.

Through the use of the dielectric function, this definition offers us a convenient, flexible, and general way to compute the fluctuation potential needed to evaluate the cross section of plasmon peaks for any type of material and dimensionality. Moreover, being based on a proper description of the dielectric function, it makes a direct connection with the PEELS method developed by Godet, David, and coworkers [4,5], thereby reinforcing their idea that this spectroscopy could be used ultimately to map somehow the bulk or surface dielectric functions.

It is not the purpose of this article to implement the calculation of the plasmon peak. This will be done in a forthcoming study. Rather here, we dedicate our work to reviewing and documenting different models of dielectric functions in order to assess their sensitivity to various parameters. In this view, we remark that some spectroscopies such as photoemission do not resolve the momentum of the plasmon and therefore will need to integrate over it, while others such as electron energy loss spectroscopy (EELS) are plasmon momentum sensitive, at least for small values of \mathbf{q} .

Ideally, we could obtain the dielectric function from an *ab initio* electronic structure calculation.

Some codes can do it for nonzero \mathbf{q} values, but as ultimately the dielectric function will be embedded into an optimization loop as an external parameter that can be varied (think of PEELS), we have developed a separate, simplified (approximate) computer code that can compute it in a matter of seconds. This code, which is called MsSpec-DFM (dielectric function module), will be published as a separate module of MsSpec [12,13]. It can compute different model dielectric functions for a very large range of materials. The purpose of this article is to compare different approaches to analytically model a dielectric function and try to ascertain the most accurate. All the methods we use are based either on the homogeneous gas approach or on a Fermi liquid one. This means that the electron system that responds to the sudden appearance of either a core hole or a photoelectron has no structure whatsoever. Later, in a forthcoming work, we will try to assess the effect of the band structure (nonhomogeneous distribution of electrons) and of the crystal structure (interaction with phonons) on the plasmon description. Work is currently in progress using the Questaal LMTO code [17] to model a band-structure-sensitive plasmon dispersion [18], and preliminary results are very promising.

In Sec. II, we recall the basics of the Hedin-Fujikawa quasiboson multiple scattering description of the plasmon photoemission peak. Section II A describes the theoretical context of the multiple scattering of spectroscopies, while Sec. II B introduces the quasiboson model Hamiltonian. Section II C introduces the fluctuation potential, and Sec. II D the essentials on dielectric function formulation. Section III is devoted to the description of various model dielectric functions encompassing (i) the simple plasmon pole approximation, (ii) the random phase approximation (RPA) approximation, and (iii) the correlation-augmented RPA approximations. As these models do not conserve the number of particles, we consider in Sec. IV two approximations that ensure this conservation: (i) the Mermin approximation and (ii) the Hu-O'Connell approximation. More refined methods that also conserve the momentum and the energy such as the Atwal-Ashcroft method [19] are not tested here because they can be easily implemented into the family of dielectric functions described in Sec. V. Section V deals with a more unusual pathway to build up a dielectric function. Indeed, as we mentioned before, most standard model dielectric functions do not conserve the number of particles. In addition, the RPA does not contain correlation effects and they have to be added externally through local field corrections (LFCs). It can be shown however that the ω^1 moment of the inverse of the dielectric function is nothing else than an expression of the conservation of the number of particles. Likewise the ω^3 moment can be shown to reflect the electron pair correlations [20] and the ω^5 moment the electron triplet correlations [21]. Consequently, if we can reconstruct the dielectric function, or its inverse, from its moments, we will have “built-in” both the conservation of the number of particles and the correlations. We document here two methods based on this approach: (i) the Nevanlinna function method and (ii) the memory function method. We show that these two methods do improve upon the correlation-augmented RPA methods or the damping methods (Mermin, Hu-O'Connell). In addition, complex energies can be used that incorporate plasmon damping. Although in this article we will limit ourselves to the scalar memory function approach, we note that it can be augmented to a matrix version that will incorporate the conservation of the momentum and the conservation of the energy. As the memory function is based on the way a system relaxes, other features, such as the timescales of different plasmon decay modes, can also be added into the memory matrix method which makes it the most flexible and general way to model “analytically” a dielectric function. Furthermore, it can be shown that most, if not all, other methods can be considered as particular cases. A comparative discussion is proposed in Sec. VI.

Note that throughout this article, we consider the case of aluminum for our calculations. This particular choice comes from the fact that aluminum is a much studied system usually considered as a test case, or toy model.

II. THEORETICAL BACKGROUND

A. Spectroscopies and multiple scattering

The form of multiple scattering (MS) used in spectroscopy codes nowadays has a long history that dates back to the late

1940s and early 1950s and the seminal articles by Korringa [22] and Kohn and Rostoker [23]. It was conceived as a method to solve the bound-state electronic structure problem and it is still known now under the acronym KKR, made from the initials of the three authors. Later, it was extended to treat continuum states, which allowed one to apply it to the description of spectroscopies involving electrons. In this case, it is called more often multiple scattering, a generic name that is used also in other areas of physics. Indeed, many important results of multiple scattering have been first demonstrated in nuclear physics and then rediscovered in condensed matter.

For the case of the present work, we are interested to embed the description of plasmon satellites in spectroscopies within this multiple scattering formalism. Let us take the case of photoemission as an example. A core-state peak in the overall spectrum can be modeled as

$$I^0(\mathbf{k}, \hbar\omega) \propto |\langle \tilde{\phi}_{\mathbf{k}} | \Delta | c \rangle|^2. \quad (3)$$

Here, $|c\rangle$ is the core state excited by a photon of energy $\hbar\omega$, Δ is the photon-electron interaction operator, usually reduced its dipole part, and $|\tilde{\phi}_{\mathbf{k}}\rangle$ is the continuum multiple scattering wave state of the escaping electron with momentum \mathbf{k} . This continuum state contains all the interactions of the excited electron with the atoms of the material before detection by the analyzer. Although it usually incorporates a description of inelastic losses through a suitable optical potential, it cannot account for plasmon losses which appear in the spectrum as separate satellite peaks. Hence, a supplementary theoretical model is needed for such a description.

B. The quasiboson approximation

As already mentioned in the introduction, Hedin and his coworkers introduced two separate frameworks to incorporate plasmons into photoemission and x-ray absorption: the GW + cumulant expansion, and the quasiboson model Hamiltonian [6–8].

In Hedin’s quasiboson model Hamiltonian method [15,24,25], the coupling to the plasmon field is added externally and treated as a perturbation. This allows one to embed it easily into the MS formalism.

In our case, the quasiboson model Hamiltonian can be written as

$$\begin{aligned} H = & \sum_{\mathbf{q}} \hbar\omega_{\mathbf{q}} b_{\mathbf{q}}^{\dagger} b_{\mathbf{q}} + \sum_{\mathbf{k}} \epsilon_{\mathbf{k}} c_{\mathbf{k}}^{\dagger} c_{\mathbf{k}} \\ & + \sum_{\mathbf{q}\mathbf{k}\mathbf{k}'} [V_{\mathbf{k}\mathbf{k}'}^{\mathbf{q}} b_{\mathbf{q}}^{\dagger} + (V_{\mathbf{k}\mathbf{k}'}^{\mathbf{q}})^* b_{\mathbf{q}}] c_{\mathbf{k}}^{\dagger} c_{\mathbf{k}'} - \sum_{\mathbf{q}} V_{cc}^{\mathbf{q}} (b_{\mathbf{q}} + b_{\mathbf{q}}^{\dagger}), \end{aligned} \quad (4)$$

where the first term describes the free boson field, the second term corresponds to the ejected photoelectron, and the third term corresponds to the interaction between the photoelectron and the boson field. The last term represents the core hole–boson coupling. In this approach, the interaction between an external charge and the electrons in the system is described through the fluctuation potential $V^{\mathbf{q}}$ given by Eq. (2) where, specializing to plasmons, $\hbar\omega_{\mathbf{q}}$ is the excitation energy of a plasmon of momentum \mathbf{q} . The momentum vector of a plasmon is given by $\mathbf{q} = \mathbf{k}_{\text{in}} - \mathbf{k}_{\text{sc}}$ where \mathbf{k}_{in} is the momentum of the

electron before the plasmon loss and \mathbf{k}_{sc} is the momentum of the electron after the plasmon loss.

In their respective works, Hedin and coworkers and Fujikawa and coworkers relied on two analytical fluctuation potentials developed separately by Bechstedt [16] and Inglesfield [26], which we will describe later for the sake of completeness.

In the Hedin-Fujikawa formalism, the intensity of the first plasmon peak is given by [11]

$$I^1(\mathbf{k}, \hbar\omega, \hbar\omega_{\mathbf{q}}) = I^0(\mathbf{k}, \hbar\omega) \frac{\alpha(\hbar\omega_{\mathbf{q}})}{\hbar\omega_{\mathbf{q}}}, \quad (5)$$

where \mathbf{k} is the momentum of the detected electron, and \mathbf{q} that of the plasmon. The “no-loss” core-peak cross section is [11]

$$\begin{aligned} I^0(\mathbf{k}, \hbar\omega) = & 4\pi^2 \alpha_{\text{FS}} \frac{\hbar}{m^2 \omega} |\langle \tilde{\phi}_{\mathbf{k}} | \Delta | c \rangle|^2 \\ & \times \exp \left[- \int_0^{+\infty} \frac{\alpha(\epsilon)}{\epsilon} d\epsilon \right]. \end{aligned} \quad (6)$$

The term before the multiplication sign is the usual core-level cross section which is computed by standard MS codes such as MsSpec [12,13]. α_{FS} is the usual fine-structure constant. The last term results from an overlap matrix element and is often neglected.

Within the Hedin-Fujikawa formalism, the loss function $\alpha(\epsilon)/\epsilon$ can be expressed as

$$\frac{\alpha(\epsilon)}{\epsilon} = \sum_{\mathbf{q}} \left| \int f_c(\mathbf{r}) V^{\mathbf{q}}(\mathbf{r}) d\mathbf{r} \right|^2 \delta(\epsilon - \hbar\omega_{\mathbf{q}}), \quad (7)$$

where $f_c(\mathbf{r})$ is a well-defined core-state related function and $V^{\mathbf{q}}(\mathbf{r})$ is the fluctuation potential corresponding to the excitation of a plasmon of energy $\hbar\omega_{\mathbf{q}}$. So, for quantitative modeling of plasmon features in spectroscopies it is imperative to have a good fluctuation potential as it is the only unknown in Eq. (7). For $V^{\mathbf{q}}(\mathbf{r})$ both Hedin and Fujikawa have used the analytical expressions derived either by Inglesfield [14] or by Bechstedt [15,16]. As already described in the introductory section, these two fluctuation potentials have strong limitations due to the fact that (i) they have been derived for metals only, and (ii) they are surface related.

C. Fluctuation potentials

The fluctuation potential describes the coupling between the electron and the bosons. It is not the purpose of this article to go into the details of the analytical derivation of the ones that can be found in the literature. From Eq. (2), we see that it can be factorized as

$$V^{\mathbf{q}}(\mathbf{r}) = V^{\mathbf{q}} e^{i\mathbf{q}\cdot\mathbf{r}}. \quad (8)$$

The different models of analytical fluctuation potentials available in the literature have been obtained within linear response theory. In addition, in the case of Inglesfield and Bechstedt, the choice of a semi-infinite electron gas implies that the exponential in (8) reduces essentially to the form $\exp[\mathbf{q}_{\parallel}z]$. In the following, $\omega(\mathbf{q})$ is the plasmon dispersion, and ω_p is the plasmon (threshold) frequency, which can be obtained from the constant density \bar{n} of the electron gas.

1. Plasmon pole

The plasmon pole fluctuation potential was originally derived by Lundqvist [19]. Its value is

$$V^{\mathbf{q}}(z) = V_{\text{PP}}^{\mathbf{q}} e^{i\mathbf{q}\cdot\mathbf{r}},$$

$$V_{\text{PP}}^{\mathbf{q}} = \sqrt{V_C(\mathbf{q}) \frac{\omega_p^2}{\omega(\mathbf{q})} \frac{1}{2V}},$$

where $V_{\text{PP}}^{\mathbf{q}}$ is the electron plasmon coupling constant and V is the system volume. For the surface case, we replace the 3D Fourier transformation of the bare Coulomb potential $V_C(\mathbf{q})$ by the 2D transformation and take into account that \mathbf{q} is parallel to the surface. It is easy to verify that the application of Eq. (2) to the plasmon pole dielectric function allows one to recover Lundqvist's result.

2. Inglesfield

Inglesfield introduced a more realistic analytical potential, using the fact that the bulk modes in a semi-infinite system are standing waves, i.e., phase-shifted cosines modified at the surface [26]. The Inglesfield bulk plasmon potential is given as

$$V^{\mathbf{q}}(z) = V_{\text{IN}}^{\mathbf{q}} [\cos(-q_z z + \phi_{\mathbf{q}}) - e^{q_{\parallel} z} \cos \phi_{\mathbf{q}}] \theta(z), \text{ inside,}$$

$$= 0, \text{ outside,} \quad (9)$$

where

$$V_{\text{IN}}^{\mathbf{q}} = \sqrt{\frac{\omega_p^2}{\omega(\mathbf{q})} \frac{1}{V} V_C(\mathbf{q})},$$

$$\phi_{\mathbf{q}} = \tan^{-1} \left(\frac{q_{\parallel}}{q_z} \right). \quad (10)$$

Similarly, the Inglesfield surface plasmon potential is given as

$$V^{\mathbf{q}}(z) = V_{\text{IN}}^{\mathbf{q}} e^{q_{\parallel} z},$$

$$V_{\text{IN}}^{\mathbf{q}} = \sqrt{V_C^{2D} \frac{\omega_p}{A\sqrt{8}}}. \quad (11)$$

A is the area of the surface, with the Coulomb potential Fourier transforms being

$$V_C = V_C^{2D} = \frac{e^2}{2\epsilon_0 \sqrt{q^2 + k_s^2}}, \quad (12)$$

where k_s is a screening momentum.

3. Bechstedt

Bechstedt and coworkers derived an expression for the screened potential W . It was recast in terms of the fluctuation potential by Hedin and coworkers [15]:

$$V^{\mathbf{q}}(z) = N_b [e^{q_{\parallel} z} \theta(z) + \{(2 + C_1 + C_3) \cos(q_z z) - C_2 \sin(q_z z) - (1 + C_1) e^{q_{\parallel} z} - C_3 \exp(\sqrt{\omega_p + \omega(\mathbf{q}) + q_{\parallel}^2} z)\} \theta(-z)], \quad (13)$$

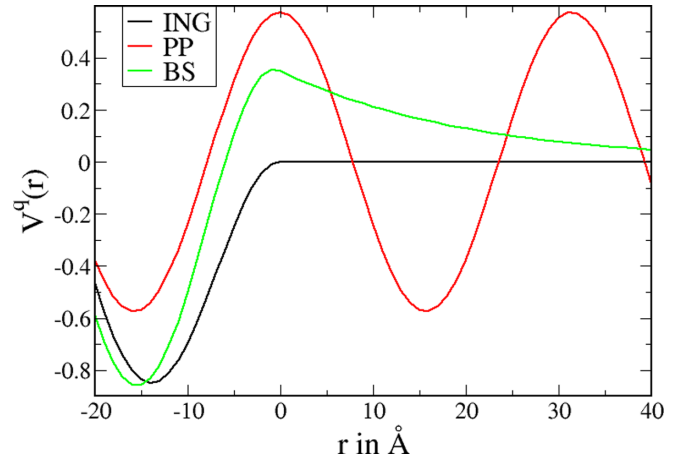


FIG. 1. Radial variations of the standard analytical fluctuation potentials. Red: Plasmon pole (PP); black: Inglesfield (ING); green: Beschstedt (BS).

where the coefficients are given by

$$C_1 = \frac{\omega_p^2}{\omega(\mathbf{q})^2 - \omega_p^2},$$

$$C_2 = -\frac{q_{\parallel} \omega_p^2}{2\omega(\mathbf{q})[\omega(\mathbf{q}) - \omega_p] q_z},$$

$$C_3 = -\frac{q_{\parallel} \omega_p^2}{2\omega(\mathbf{q})[\omega(\mathbf{q}) + \omega_p] q_z \sqrt{\omega_p + \omega(\mathbf{q}) + q_{\parallel}^2}}. \quad (14)$$

In the surface case,

$$V^{\mathbf{q}}(z) = N_s [e^{-q_{\parallel} z} \theta(z) + a(q_{\parallel}, z, \omega) \theta(-z)]. \quad (15)$$

$a(q_{\parallel}, z, \omega)$ is related to the bulk dielectric function through [16]

$$a(q_{\parallel}, z, \omega) = \frac{2q_{\parallel}}{\pi} \int_0^{\infty} \frac{\cos(q_z z)}{q^2 \epsilon(\mathbf{q}, \omega)} dq_z, \quad (16)$$

where $\epsilon(\mathbf{q}, \omega)$ can be computed within the simple plasmon pole model.

These three potentials are the standard analytical fluctuation potentials available in the literature. Their space variations are represented in Fig. 1, for the aluminum case. However, due to the fact that they are surface related (and derived for metals), they cannot be used to describe spectra derived for reduced-symmetry systems such as quantum dots, quantum wells, graphene and other 2D materials, Dirac materials, etc. In addition, they are not suited to high-energy spectroscopies such as HAXPES where the surface can be safely ignored.

In order to overcome the limitations of these potentials, we will go back to Hedin's definition of the fluctuation potential [Eq. (2)], which expresses this potential as a function of the dielectric function. This will allow us a much more flexible approach where the true dimensionality and structure of the material can be properly taken into account.

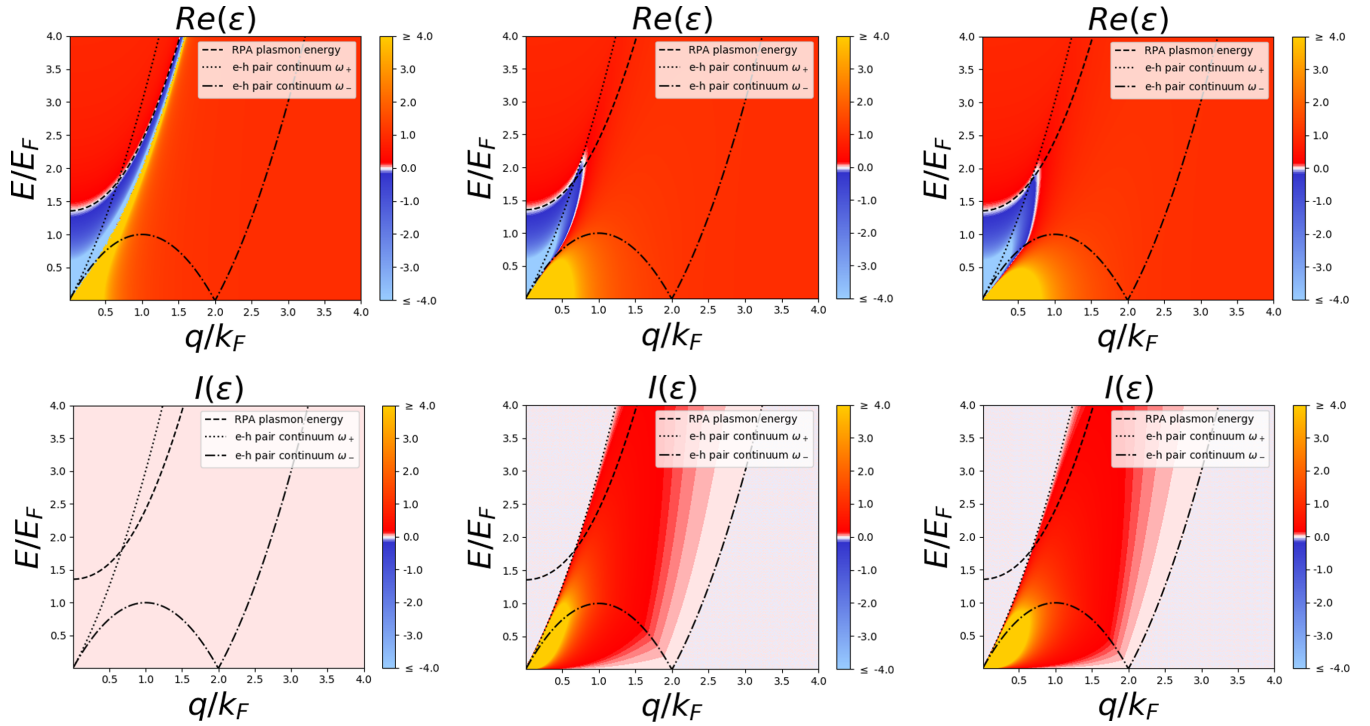


FIG. 2. Real (above) and imaginary (below) part of dielectric function $\epsilon(\mathbf{q}, \omega)$ for (left) plasmon pole, (center) RPA, (right) RPA + UTI1. UTI1 incorporates the Utsumi-Ichimarui static local field corrections. The dashed line is the RPA analytical approximate dispersion curve computed up to q^4 . It serves as a guideline to the eyes. The exact plasmon dispersion for a given model corresponds to the upper white band. The space between the ω^+ (dotted line) and ω^- (dash-dotted line) parabolas is the so-called Landau region where electron-hole pairs are excited.

D. Dielectric function: General background

The dielectric function of a system describes the response of this system to an external perturbation. It is determined by the properties of the system and its interaction with the perturbing object. Several related quantities can be found in the literature, together with their relationship with various spectroscopies. For instance, it is well known that the cross section of the EELS is related to the loss function. Therefore, in the following subsection, we will introduce the different quantities of interest for spectroscopies and their relation to the dielectric function.

We start by decomposing the dielectric function into its real and imaginary parts,

$$\epsilon(\mathbf{q}, \omega) = \epsilon_1(\mathbf{q}, \omega) + i\epsilon_2(\mathbf{q}, \omega). \quad (17)$$

Then, the loss function $L(\mathbf{q}, \omega)$ is related to the dielectric function of the solid through

$$L(\mathbf{q}, \omega) = \text{Im} \left[\frac{-1}{\epsilon(\mathbf{q}, \omega)} \right] = \frac{\epsilon_2(\mathbf{q}, \omega)}{|\epsilon(\mathbf{q}, \omega)|^2}. \quad (18)$$

Similarly, in the case of 3D systems at $T = 0$, the dynamical structure factor can be expressed as [27]

$$S(\mathbf{q}, \omega) = \frac{\hbar}{\pi} \frac{1}{\bar{n}} \frac{1}{V_C(\mathbf{q})} \text{Im} \left[\frac{-1}{\epsilon(\mathbf{q}, \omega)} \right]. \quad (19)$$

As before, $V_C(\mathbf{q})$ is the Fourier transform of the Coulomb potential and \bar{n} the constant electron density. It describes the spectrum of excitations in the system as a function of the momentum transfer \mathbf{q} and the energy transfer.

Likewise, the susceptibility, or density-density response function, can be defined as

$$\chi(\mathbf{q}, \omega) = \frac{1}{V_C(q)} \left[\frac{1}{\epsilon(\mathbf{q}, \omega)} - 1 \right]. \quad (20)$$

With these tools, we can access many different ways to model the dielectric function, and compute cross sections.

The simplest case: Plasmon pole

The plasmon pole dielectric function describes the response of the system entirely in terms of collective modes. The dielectric function is just the analytic continuation of a simple pole and is given by [28]

$$\epsilon(\mathbf{q}, \omega) = 1 - \frac{\omega_p^2}{\omega^2 + \omega_p^2 - \omega(\mathbf{q})^2}. \quad (21)$$

Here, $\omega(\mathbf{q})$ is the plasmon dispersion and ω_p the plasmon frequency. The real part and imaginary part of $\epsilon(\mathbf{q}, \omega)$ are represented in Fig. 2 for the case of aluminum.

The plasmon dispersion band corresponds to the upper band of $\text{Re}[\epsilon(\mathbf{q}, \omega)] = 0$, in white on the figures.

III. RPA AND BEYOND

The plasmon pole approximation's main drawback, as can be seen from the left-hand part of Fig. 2, is that it does not incorporate any damping mechanism. Therefore, we have a plasmon [the upper white band in the real part of $\epsilon(\mathbf{q}, \omega)$] which, once created, never decays. This is clearly not

physical. Historically, the first expression of the dielectric function to include a damping mechanism is the random phase approximation (RPA) originally derived by Lindhard [29]. This approximation is based on the description of the delocalized electron system as a *homogeneous and noninteracting electron gas*. The real and imaginary parts of the RPA dielectric function are represented in the middle figure of Fig. 2. The region comprised between the two parabolas ω_+ and ω_- is the region where excitation of single electron-hole pairs is allowed. It is called the Landau region. We see clearly now that we have damping into this region. Therefore, this damping comes from the decay of the plasmon into an electron-hole pair. There is however no damping mechanism built-in outside the Landau region, which means that there, the plasmon will “live” forever. In addition, being built on the assumption that the electron gas is noninteracting, the RPA does not allow for correlation effects.

Correlation effects can be introduced into the RPA through the so-called *local field corrections* (LFCs) $G(\mathbf{q}, \omega)$. These corrections are related to the exchange and correlation term of density functional theory (DFT). For a given correction term, the correlation-augmented dielectric function can be written as

$$\varepsilon(\mathbf{q}, \omega) = \frac{V_C(\mathbf{q})\Pi^{\text{RPA}}(\mathbf{q}, \omega)}{1 + V_C(\mathbf{q})G(\mathbf{q}, \omega)\Pi^{\text{RPA}}(\mathbf{q}, \omega)}, \quad (22)$$

where $G(\mathbf{q}, \omega)$ is the dynamical local field correction. The RPA dielectric function is given by

$$\varepsilon^{\text{RPA}}(\mathbf{q}, \omega) = 1 - V_C(\mathbf{q})\Pi^{\text{RPA}}(\mathbf{q}, \omega), \quad (23)$$

where $\Pi^{\text{RPA}}(\mathbf{q}, \omega)$ is the RPA polarization.

Very few models of *dynamical* local field corrections exist in the literature, while a lot of attention has been devoted to *static* corrections $G(\mathbf{q})$. Therefore, we will restrict ourselves here to the latter.

In order to investigate the effect of such corrections on the behavior of the dielectric function, we consider here three different types of static corrections, the Hubbard model (HUBB), which takes only into account the exchange effect, the Pathak-Vashista correction (PVHF) [20], and the Utsumi-Ichimarū (UTII) one [30]. They can be expressed respectively as

$$\begin{aligned} G(\mathbf{q})_{\text{HUBB}} &= \frac{1}{2} \frac{x^2}{1+x^2}, \\ G(\mathbf{q})_{\text{PVHF}} &= \frac{1}{\omega_p^2} J(q), \\ G(\mathbf{q})_{\text{UTII}} &= \frac{3(4-x^2)(28+5x^2)}{16x} \times \ln \left| \frac{2+q}{2-q} \right|, \end{aligned} \quad (24)$$

where we have used the notation $x = q/k_F$. Here, $J(q)$ is the Kugler function [31]

$$J(q) = \frac{e^2}{m\pi} \int_0^{+\infty} k^2 [S(k) - 1] J(k, q) dk, \quad (25)$$

where $J(k, q)$ is given by

$$J(k, q) = \frac{5}{6} - \frac{k^2}{2q^2} + \frac{q}{4k} \left(\frac{k^2}{q^2} - 1 \right)^2 \ln \left| \frac{k+q}{k-q} \right|. \quad (26)$$

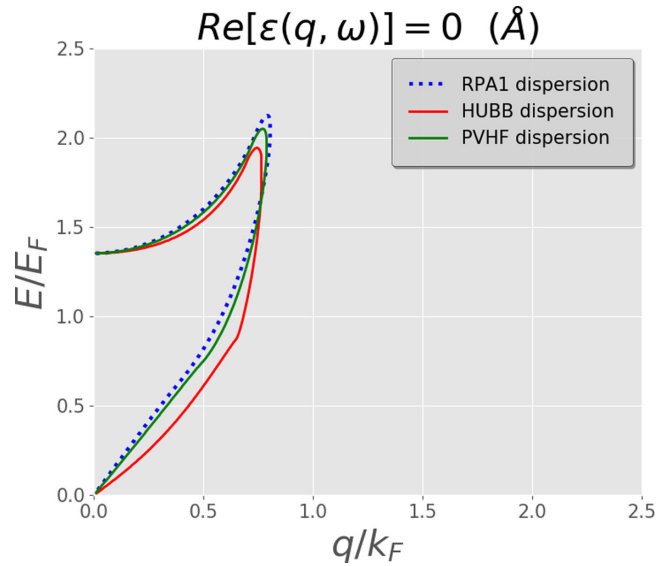


FIG. 3. Comparison of collective excitation dispersion lines for RPA and some RPA + local field corrections. The plasmon dispersion corresponds to the upper band. We note very few differences between the dispersion bands.

$S(q)$ is the static structure factor. Here, we approximate it by its Hartree-Fock value

$$\begin{aligned} S_{\text{HF}}(q) &= \frac{3}{4} \frac{q}{k_F} - \frac{1}{16} \left(\frac{q}{k_F} \right)^3, \quad \text{for } q < 2k_F, \\ &= 1, \quad \text{for } q > 2k_F. \end{aligned} \quad (27)$$

The right-hand plots of Fig. 2 correspond to the real part (up) and imaginary part (down) of the UTII-enhanced RPA dielectric function. We see clearly a change in the dispersion of the collective excitations (white band), with respect to the RPA case. The comparison between this dispersion is even clearer in Fig. 3 where we give a 2D representation of the collective excitation bands for the RPA, RPA + Hubbard, and RPA + Pathak – Vashista static local field corrections. Nevertheless, even if we now incorporate correlation effects into the dielectric function, we see clearly that, despite some minor changes in the imaginary part of the dielectric function (see Fig. 2), we are still unable to properly describe plasmon damping outside the Landau regime. In principle, we could go to dynamic LFCs, but in the following, we will rather explore completely other ways to describe the dielectric function with built-in damping.

IV. DAMPING-BASED DIELECTRIC FUNCTIONS

RPA alone has a certain number of limitations: (i) it fails to conserve the number of particles, (ii) it does not contain correlation effects (they have to be added externally through local field corrections), and (iii) it does not incorporate plasmon damping outside the Landau regime. In order to cure (i), Mermin [32] extended the Lindhard dielectric function in the relaxation-time approximation, where essentially the collisions relax the electronic density matrix not to its uniform equilibrium value, but to a local equilibrium density matrix.

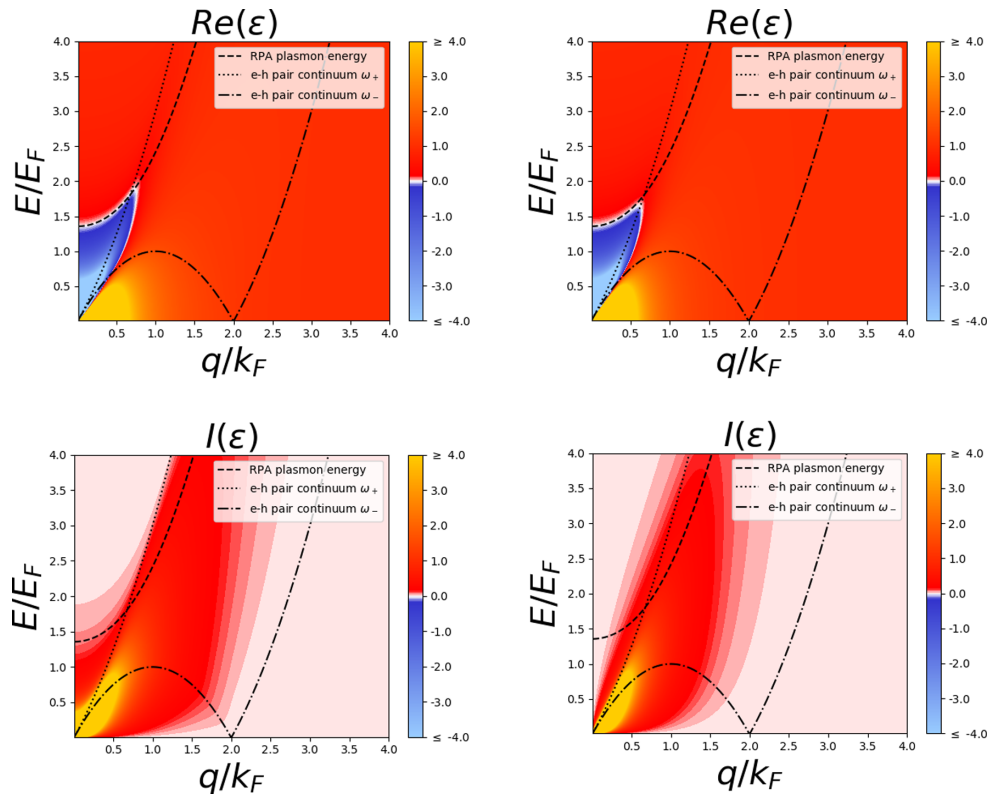


FIG. 4. Real and imaginary part of the (left) Mermin dielectric function with a relaxation time of 0.5 fs, (right) Hu-O'Connell dielectric function with a diffusion coefficient $D = 2.9 \times 10^{-5} \text{ m}^2 \text{ s}^{-1}$. Both imaginary parts exhibit damping outside the Landau region.

The Mermin [33] dielectric function thus can be written as

$$\varepsilon(\mathbf{q}, \omega) = 1 + \frac{(1 + \frac{i}{\omega\tau})[\varepsilon^0(\mathbf{q}, \omega + i/\tau) - 1]}{1 + \frac{i}{\omega\tau}[\frac{\varepsilon^0(\mathbf{q}, \omega + i/\tau) - 1}{\varepsilon^0(\mathbf{q}, 0) - 1]}}, \quad (28)$$

where $\varepsilon^0(\mathbf{q}, \omega)$ is the RPA dielectric function and $\bar{\omega} = \omega + i/\tau$ is a complex frequency incorporating damping through the relaxation time τ . Mermin's interest here is in the long-wavelength limit behavior of the electron gas where the focus is on obtaining a modified Lindhard dielectric function which reduces to the correct classical behavior in the $q \rightarrow 0$ limit.

Following the same idea, Hu and O'Connell [34] generalized the Lindhard dielectric function to include fluctuation effects arising from electron-electron and electron-impurity interactions. They also studied Friedel oscillations as an example of the application of their generalized version of the Lindhard function and observed that these oscillations are damped due to the inclusion of fluctuation effects. Due to the complexity of the Hu-O'Connell equations, which are expressed in terms of the diffusion coefficient D , we do not reproduce them here but refer instead to their article [34]. As displayed in Fig. 4, we now observe a damping in the imaginary part of both the Mermin and the Hu-O'Connell dielectric function in the non-Landau region. This damping can be regarded as the signature of a built-in lifetime for the plasmon. However, being based upon the standard RPA model, they lack a proper description of correlations.

These two approaches are encouraging, as we do need a proper damping of the plasmon in order to correctly describe the relaxation of the system. This damping is clearly absent in

the standard plasmon pole and RPA methods, even when the latter is augmented with various *static* local field corrections in order to incorporate electron-electron correlations.

V. DIELECTRIC FUNCTION: ALTERNATIVE APPROACH

An alternative family of dielectric functions can be obtained through a reconstruction from the first few moments. Two independent approaches can be found in the literature, the Nevanlinna approach [35] and the memory function approach [36]. The main advantage of these two approaches is that conservation of the number of particles and correlation are built-in. We note that for larger values of ω , $\text{Im}[\varepsilon^{-1}(\mathbf{q}, \omega)]$ tends quickly to zero, so that we have the expansion

$$\varepsilon^{-1}(\mathbf{q}, \omega) = 1 + \sum_{n=1}^{+\infty} \frac{\langle \omega^{2n-1} \rangle_L}{\omega^{2n}}. \quad (29)$$

As mentioned in the introduction, it is well known that the RPA dielectric function does not satisfy the compressibility sum rule and the frequency moment sum rules [37]. This realization is the starting point of the two above-mentioned approaches which we outline now.

A. The Nevanlinna function method

The Nevanlinna approach is based on the moments of the loss function. It has been developed essentially in the context of strongly coupled plasmas. The standard loss function described in Eq. (18) is related to the *Nevanlinna loss function*

by

$$\mathcal{L}(\mathbf{q}, \omega) = \frac{L(\mathbf{q}, \omega)}{\omega}. \quad (30)$$

The corresponding moments are defined as [35]

$$C_n = \frac{1}{\pi} \int_{-\infty}^{+\infty} \omega^{n-1} \text{Im} \left[\frac{-1}{\varepsilon(\mathbf{q}, \omega)} \right] d\omega = \frac{1}{\pi} \langle \omega^{n-1} \rangle_{\mathcal{L}}. \quad (31)$$

A dimensional analysis shows that the moment $C_2(q)$ has the dimension of a squared frequency, and likewise for every ratio $C_{n+2}(q)/C_n(q)$. Therefore, we introduce the notation

$$\omega_n^2(q) = \frac{C_{2n}(q)}{C_{2n-2}(q)}. \quad (32)$$

The $\omega_n(q)$ have the dimension of a frequency and are the characteristic frequencies in the Nevanlinna function approach. The same characteristic frequencies will appear in the memory function method. The connection between the different types of moments can be made using, for the $T = 0$ K case,

$$\begin{aligned} L(\mathbf{q}, \omega) &= \text{Im} \left[\frac{-1}{\varepsilon(\mathbf{q}, \omega)} \right] = V_C(q) \frac{\pi \bar{n}}{\hbar} S(\mathbf{q}, \omega) \\ &= -V_C(q) \text{Im}[\chi(\mathbf{q}, \omega)], \end{aligned} \quad (33)$$

where we find

$$V_C(q) \frac{\pi \bar{n}}{\hbar} = \frac{\pi}{2} \frac{\omega_p^2}{\omega_{\mathbf{q}}}, \quad (34)$$

implying

$$\langle \omega^n \rangle_S = \frac{2}{\pi} \frac{\omega_{\mathbf{q}}}{\omega_p^2} \langle \omega^n \rangle = -\frac{\hbar}{\bar{n}\pi} \langle \omega^n \rangle_{\chi}, \quad (35)$$

with \bar{n} being the number density. Here, $\omega_{\mathbf{q}} = \hbar \mathbf{q}^2 / 2m$, and should not be mixed up with the plasmon dispersion $\omega(\mathbf{q})$. Now, the frequency moments of the loss function can be written as [38]

$$\langle \omega^{2n-1} \rangle_L = 2 \int_0^{+\infty} \omega^{2n-1} \text{Im} \left[\frac{-1}{\varepsilon(\mathbf{q}, \omega)} \right] d\omega. \quad (36)$$

So, then we have

$$\begin{aligned} \langle \omega^{-1} \rangle_L &= \pi \left[1 - \frac{1}{\varepsilon(q)} \right], \text{ compressibility sum rule,} \\ \langle \omega^1 \rangle_L &= \pi \omega_p^2, \quad f\text{-sum rule,} \\ \langle \omega^3 \rangle_L &= \pi \omega_p^2 \left[\omega_{\mathbf{q}}^2 + 4 \omega_{\mathbf{q}} \frac{\langle t \rangle}{\hbar} + \omega_p^2 + J(q) \right]. \end{aligned} \quad (37)$$

$J(q)$ is the Kugler function defined in Eq. (25) and $\langle t \rangle$ is the average kinetic energy per electron.

$n = 1$ (f -sum rule) ensures the conservation of the number of particles and $n = 2$ ensures a proper account of two-body correlation effects. The structure factor $S(\mathbf{q}, \omega)$ for a nonzero temperature system can be obtained from the loss function through the fluctuation-dissipation theorem

$$\text{Im} \left[\frac{-1}{\varepsilon(\mathbf{q}, \omega)} \right] = \frac{\pi \bar{n}}{\hbar} V_C(\mathbf{q}) \left[1 - \exp \left(-\frac{\hbar \omega}{k_B T} \right) \right] S(\mathbf{q}, \omega). \quad (38)$$

For low energies, or large temperatures, this can be approximated by

$$\text{Im} \left[\frac{-1}{\varepsilon(\mathbf{q}, \omega)} \right] \approx \frac{\pi \bar{n}}{k_B T} V_C(\mathbf{q}) \omega S(\mathbf{q}, \omega). \quad (39)$$

The Nevanlinna method is mathematically involved. It relies on the mathematical solution of the so-called *noncanonical solution of the Hamburger moment problem*. It is not the purpose of the present article to go into the details of the method. We refer the readers interested by this approach to the review article by Tkachenko [39]. The main point is that it involves a reconstruction of the dielectric function in terms of characteristic frequencies ω_n that are functions of the first moments of the loss function. Building up on the mathematical theorems, one arrives at the equation

$$\begin{aligned} \varepsilon^{-1}(\mathbf{q}, \bar{\omega}) &= 1 + \frac{\omega_p^2 [\bar{\omega} + Q_2(\mathbf{q}, \bar{\omega})]}{\bar{\omega}(\bar{\omega}^2 - \omega_2^2) + Q_2(\mathbf{q}, \bar{\omega})(\bar{\omega}^2 - \omega_1^2)} \\ &\quad \times \text{Im}[\bar{\omega}] \geq 0 \end{aligned} \quad (40)$$

for the 3-moment expression. Here, ω_p is the plasmon frequency, $Q_2(\mathbf{q}, \bar{\omega})$ is the *unknown* Nevanlinna function, and $\bar{\omega}$ is the complex frequency whose imaginary part represents the plasmon damping. We note that $Q_2(\mathbf{q}, \bar{\omega})$ has the dimension of a frequency.

In an electron liquid, the Nevanlinna function plays the role of the *dynamical* local field correction $G(\mathbf{q}, \omega)$. More precisely, we have [40]

$$\begin{aligned} G(\mathbf{q}, \bar{\omega}) &= 1 + \frac{1}{[\varepsilon_{\text{RPA}}(\mathbf{q}, \bar{\omega}) - 1]} + \frac{\bar{\omega}^2}{\omega_p^2} \\ &\quad - \frac{\bar{\omega} \omega_2^2 + \omega_1^2 Q_2(\mathbf{q}, \bar{\omega})}{\omega_p^2 [\bar{\omega} + Q_2(\mathbf{q}, \bar{\omega})]}. \end{aligned} \quad (41)$$

Nevanlinna functions must fulfill a number of mathematical properties including having a Riesz-Herglotz representation [39,41]. Therefore, finding relevant functions is a complex mathematical problem that has led to several papers in the literature [39,40,42,43]. Here, we make the choice [43]

$$Q_2(\mathbf{q}, \bar{\omega}) = i \frac{\pi}{2} \varepsilon(q) [\varepsilon(q) - 1] (q a_0) \omega_{\mathbf{q}} \left[\frac{\omega_2^2}{\omega_1^2} - 1 \right], \quad (42)$$

which is well suited to our needs. a_0 is the Bohr radius and we choose the RPA value for the *static* dielectric function $\varepsilon(q)$.

From Fig. 5, we observe that the correlations are properly taken into account (there is a dramatic change into the plasmon dispersion with respect to RPA-based methods) and in the imaginary part of the Nevanlinna dielectric function we see some damping of the plasmon outside the Landau region, especially along the plasmon dispersion line.

B. The memory function method

The derivation of the memory function is quite involved so that we describe here only the different steps necessary in order to arrive to the final result. For a detailed derivation, we refer the reader to some review articles [44–46]. This approach was pioneered by Zwanzig [47] and Mori [48] who built the memory function framework upon Kubo's nonequilibrium statistical physics. The starting point is to divide the

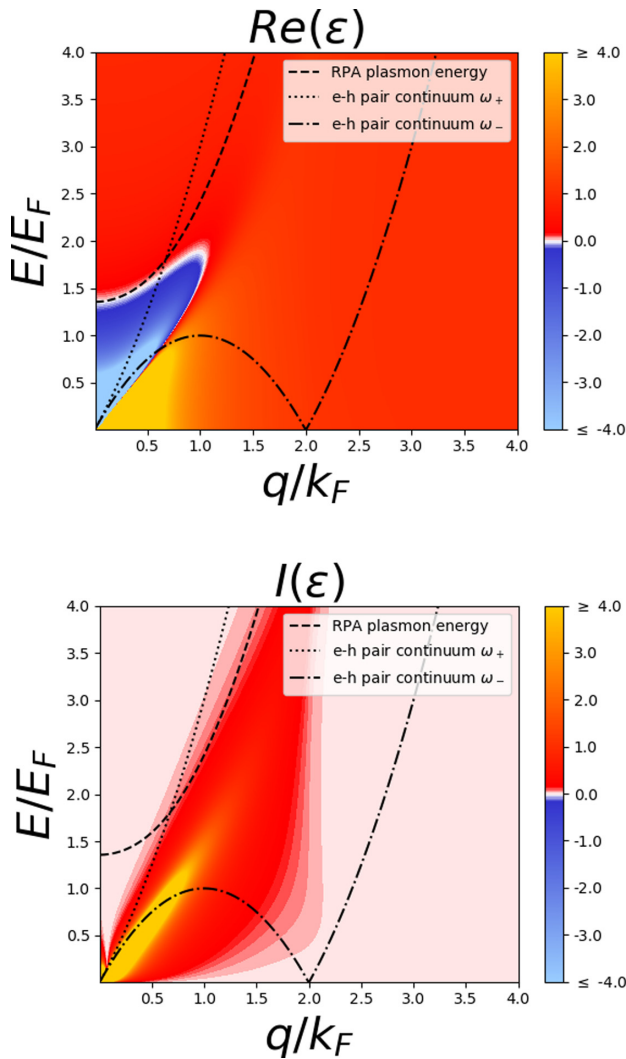


FIG. 5. Real and imaginary part of the 3-moment Nevanlinna dielectric function within the static approximation STA3. The real part shows a plasmon dispersion different compared to RPA-based methods and some damping is observed along the dispersion band outside the Landau region.

variables' space into two subspaces, that of slowly moving ones, the so-called conservative quantities, that will affect the macroscopic experimental signal, and that of fast-moving ones (nonconservative), which are not expected to impact the experimental signals. The memory function method includes the effect of the fast variables into the dynamics of the slow variables. In order to do this, we work with time-correlation functions or response functions. The connection to the dielectric function is made through the realization that (i) the dynamical structure factor $S(\mathbf{q}, \omega)$ is the time-Fourier transform of the *classical* density autocorrelation function, and (ii) the density-density response function $\chi_{nm}(\mathbf{q}, \omega)$ is related to the dielectric function [see Eq. (20)].

The next step is to show that within this variable space partitioning, autocorrelation functions satisfy an integro-differential generalized Langevin equation (GLE)

$$\frac{dC_A(t)}{dt} = - \int_0^t K_A(t-s)C_A(s)ds \quad \text{with} \quad C_A(0) = 1, \quad (43)$$

where $C_A(t)$ is the autocorrelation function of the variable A of interest, and the unknown function $K_A(t)$ is the so-called memory function which keeps track of what happened to the system before the present time t . The response function $\chi_{AA}(t)$ is related to the autocorrelation function through

$$\chi_{AA}(t) = \frac{dC_A(t)}{dt} (A|A),$$

where (A, B) is the so-called *Kubo scalar product*.

The usual Langevin equation of Brownian motion corresponds to the Markovian choice $K_A(t) = 1/\tau \delta(t)$ where at t , the dynamics of the system does not depend on the previous states of the system. The integral term containing $K_A(t)$ describes the influence of the fast-moving variables, presumably out of reach to the experiment, on the (conservative) variable A of interest.

It can be demonstrated that the memory function is also an autocorrelation function, and as such it satisfies a hierarchy of similar GLE

$$\frac{dK_n(t)}{dt} = - \int_0^t K_{n+1}(t-s)K_n(s)ds, \quad (44)$$

where we use the notation $C_A(t) = K_0(t)$ and $K_A(t) = K_1(t)$.

The next step is to take the Laplace transform of the integro-differential GLE in order to change it into an easily solvable equation. This leads to the continued fraction expansion

$$\bar{C}_A(z) = \frac{K_0(0)}{z + \frac{K_1(0)}{z + \frac{K_2(0)}{z + \frac{K_3(0)}{\dots}}}} \quad (45)$$

Truncating to order 3 (i.e., expressing the result in terms of 3 moments) and going to the response function representation gives

$$\bar{\chi}_A^{(3)}(z) = - \frac{\Delta_0^2 \Delta_1^2 [z + \bar{K}_3(z)]}{z^3 + z^2 \bar{K}_3(z) + z(\Delta_1^2 + \Delta_2^2) + \Delta_1^2 \bar{K}_3(z)}, \quad (46)$$

where the Δ_n , which have the dimension of a frequency, are functions of the moments $\langle \omega^{2n-1} \rangle_\chi$ and $K_n(0) = \Delta_n^2$. Here, $\bar{K}_3(z)$ is the Laplace transform of the memory function $K_3(t)$.

As the moments for $n = 0, 1, 2$ are well known (and to some extent, making use of some approximations, $n = 3$), the only unknown is the memory function $\bar{K}_3(z)$. Then, we have, taking A as the (constant) particle density \bar{n} ,

$$\varepsilon^{-1}(\mathbf{q}, \omega) = 1 + \frac{\omega_p^2 [\omega + i\bar{K}_3(-i\omega)]}{\omega [\omega^2 - \omega_2^2] + i\bar{K}_3(-i\omega) [\omega^2 - \omega_1^2]}. \quad (47)$$

We note that under the exchange $Q_2(\omega) \rightsquigarrow i\bar{K}_3(-i\omega)$, this equation transforms into the Nevanlinna equation (40). The difference is that we have now a physically motivated function \bar{K}_3 for which many approximations exist and that is related to the relaxation of the system, and hence in the various decay mechanisms, which could, in principle, be studied experimentally.

By definition, through the use of $\langle \omega^1 \rangle_\chi$ and $\langle \omega^3 \rangle_\chi$, Eq. (47) contains the conservation of the number of particles and a proper treatment of pair correlation effects.

If we replace the autocorrelation function A in Eq. (45) by a vector \mathbf{A} containing the density, the momentum, and the

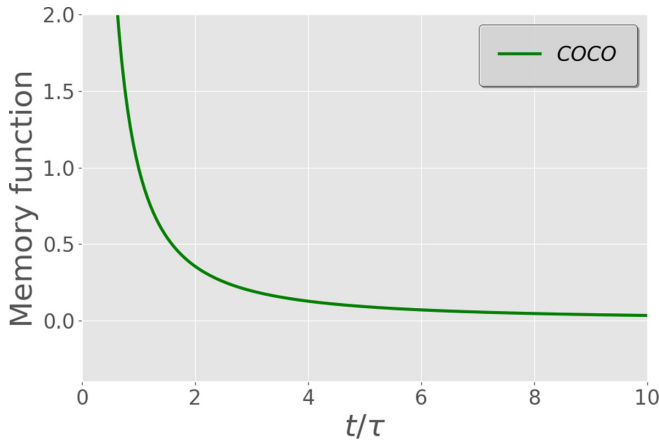


FIG. 6. The Cole-Cole (COCO) memory function $K_{CC}(t)$ in the time domain, for $\alpha = 0.5$ and $\tau = 0.5$ fs.

energy, the GLE transforms into a matrix equation [49,50]. Applying the same approach, we can derive an expression of the dielectric function that conserves the three previous quantities. This makes the memory function/memory matrix approach a very powerful and flexible tool to build up a physically meaningful dielectric function. Moreover, in case of need, two or more memory functions describing relaxations on different timescales can be used within Götze's mode-coupling formalism [51–53]. This allows one to incorporate different decay channels into the modeling of the dielectric function.

Here we consider the Cole-Cole (COCO) type memory function expression [54] for the complex dielectric function describing the relaxation process occurring in the system. This *classic* empirical model can be expressed as [54]

$$K_{CC}(t) = \tau^2 \frac{1}{\Gamma(\alpha - 1)} \left(\frac{t}{\tau}\right)^{\alpha-2} \quad (48)$$

with the power-law exponent α being $0 < \alpha \leq 1$. Here, Γ is the Gamma function. In the following, we choose $\alpha = 0.5$ and a relaxation time of $\tau = 0.5$ fs, to be consistent with the results of the Mermin dielectric function.

Figure 6 represents the behavior of the memory function in the Cole-Cole approximation as a function of time. The corresponding dielectric function is represented in Fig. 7. Here, we observe that the imaginary part of the dielectric function also shows some damping of the plasmon outside the Landau region.

VI. DISCUSSION

We have made explicit in the previous sections different ways to analytically compute model dielectric functions, starting from the simple plasmon pole and RPA, and ending up with more involved approaches involving a reconstruction in terms of the first moments. We recall that our aim in this work is to find a simple (if possible) and flexible method that would describe plasmon dispersion as accurately as possible. Indeed, our ultimate goal being to calculate plasmon fluctuation potentials in the most general possible case, we need for this to

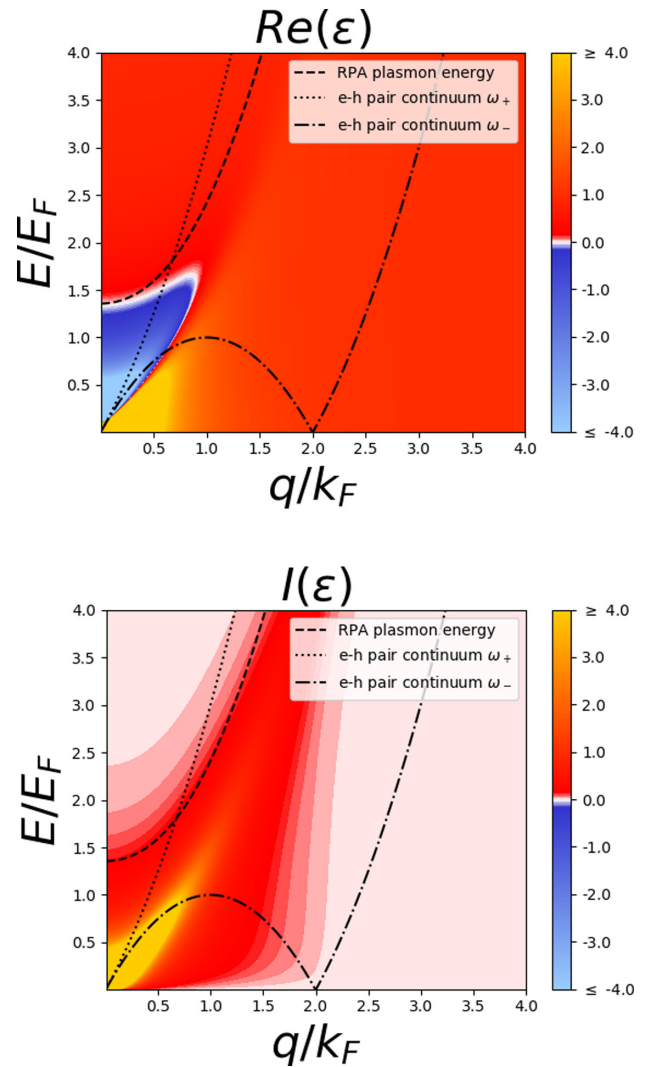


FIG. 7. Real and imaginary part of the 3-moment memory function dielectric function within the Cole-Cole approximation (COCO) for a value of $\tau = 0.5$ fs. Damping is observed all along the dispersion band outside the Landau region.

follow Hedin's definition (2),

$$V^{\mathbf{q}}(\mathbf{r}) = \left| \frac{V_C(\mathbf{q})}{\left. \frac{\partial \epsilon(\mathbf{q}, \omega)}{\partial \omega} \right|_{\omega=\omega(\mathbf{q})}} \right|^{1/2} e^{i\mathbf{q}\cdot\mathbf{r}}.$$

For low values of \mathbf{q} , the fluctuation potential will be dominated by the Coulomb part. But when \mathbf{q} increases (in photoemission, for instance, we will have to integrate over \mathbf{q} as the plasmon momentum is not detected), the features of the first derivative of the dielectric function, taken along the plasmon dispersion, will become more and more important. From this point of view, we see that two features of the dielectric function could become important: (1) the shape of the plasmon dispersion and (2) a correct description of the plasmon damping. The former corresponds to the upper band of the zeros of the real part of $\epsilon(\mathbf{q}, \omega)$ while the latter is embedded into the imaginary part.

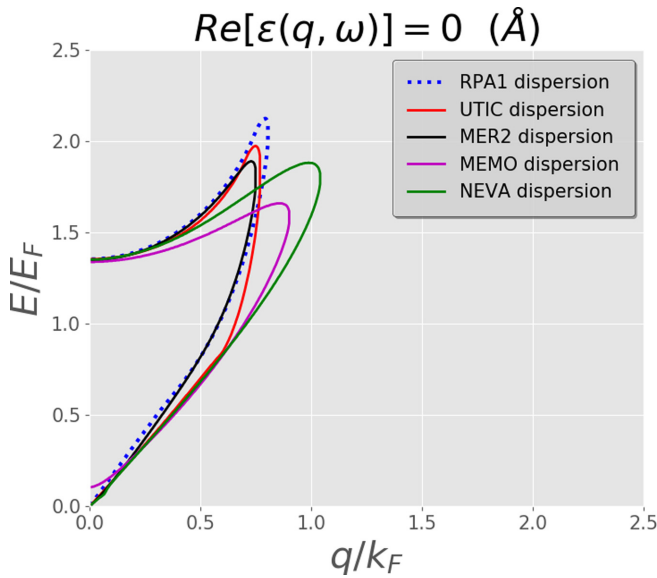


FIG. 8. Comparison of the collective excitations dispersion bands for different modeling of the dielectric function. The plasmon dispersion corresponds to the upper band. RPA1, UTIC, and MER2 correspond respectively to RPA, RPA + Utsumi – Ichimaru LFC corrections, and Mermin with $\tau = 0.5$ fs. NEVA and MEMO correspond to the Nevanlinna approach with the STA3 function, and the memory function method with the $K_{CC}(t)$ function with $\tau = 0.5$ fs.

All the calculations were done for a value of the dimensionless Wigner-Seitz radius $r_s/a_0 = 2.079$, which corresponds to aluminum ($r_s = 1.01$ Å).

From Fig. 2, we see that the plasmon pole does not exhibit any damping and that the plasmon never decays. This means that in principle, we should have to integrate q to infinity. For RPA and correlation-augmented RPA, the integration over q will be limited to a q_{\max} above which the plasmon completely decays into an electron-hole pair. This q_{\max} is very close to the intersection of the plasmon dispersion with the Landau region, which means that in practice no damping will be taken into account as clear from the imaginary-part plots.

The next types of dielectric functions we have considered are the number of electron-conserving Mermin and Hu-O’Connell ones (Fig. 4). In the former, we used a realistic value of the relaxation time $\tau = 0.5$ fs. We note that this value is about one order of magnitude larger than the approximation often made in the literature $\tau \approx 1/\omega_p$ which gives here $\tau \approx 0.04$ fs. This relaxation time approach involves the use of a complex frequency $\bar{\omega} = \omega + i/\tau$ which automatically introduces damping outside the Landau continuum. The related diffusion coefficient method (Hu-O’Connell) also gives such a damping. From this point of view, they are very appealing methods. Unfortunately, being based on the RPA, they lack a proper description of correlation effects. In the case of Mermin’s approach (see Fig. 8), this could be remedied by replacing in Eq. (28) the RPA $\epsilon^0(\mathbf{q}, \omega + i/\tau)$ by a correlation-augmented one such as RPA + UTI1.

The final approach we have documented is that based on the 3-moment reconstruction of the dielectric function. This method makes use of the moments $\langle \omega^{-1} \rangle$, $\langle \omega^1 \rangle$, and $\langle \omega^3 \rangle$

of the loss function. Here, $\langle \omega^1 \rangle$ ensures the conservation of the number of electrons while $\langle \omega^3 \rangle$ incorporates a proper treatment of pair correlations. As can be seen from Fig. 5 and Fig. 7, the more exact treatment of the correlation changes considerably the shape of the plasmon dispersion with respect to the RPA one (dotted line) or even with respect to RPA + UTI1 (Fig. 2). In addition, this type of approach does give already some damping of the plasmon outside the Landau regime. But it is noteworthy that both calculations have been done *without explicit damping*, i.e., using a real frequency ω in Eqs. (40) and (47), in contrast to the Mermin calculation that was incorporating an explicit damping in the frequency. Therefore, these two methods have even more flexibility than we have used so far.

A quantity related to the dielectric function that can be measured experimentally is the dynamical structure factor $S(\mathbf{q}, \omega)$. Lemell *et al.* [55] for instance present in their results for the dynamical structure factor derived from optical data of Mg. There, we see clearly the plasmon, starting from $q = 0$. In Fig. 9, we present the structure factors for aluminum computed from our dielectric function using the (a) RPA, (b) Mermin, (c) Nevanlinna-STA3, and (d) memory function–COCO approaches. These plots show that RPA and RPA-based dielectric functions should be ruled out as they are not able to describe properly the plasmon for low- q values, while the other methods give a much better representation that does look like the experimental results of Lemell *et al.* [55].

Now we come to the more general discussion of the choice of a suitable dielectric function model. We have not explored all the possibilities of the models, but we can already outline some important points and perspectives. The Mermin approach is limited by being RPA based, although it could be in principle expanded through the use of LFC. In addition, following the scheme devised by Götze [56] for the computation of the susceptibility, it can be demonstrated that Mermin’s dielectric function is a particular case of Götze’s scheme when neglecting correlations and using the Markovian form for the memory function $K(\omega) = 1/\tau$.

Nevanlinna functions are hard to find, but as mentioned in the memory function subsection, they are mathematically related to the memory functions through $Q_2(\omega) \rightsquigarrow i\tilde{K}_3(-i\omega)$. Moreover, following Eq. (41), we see that Nevanlinna functions and hence memory functions are strongly related to *dynamical* LFCs.

In practice, these considerations mean that most, if not all, the model dielectric functions can be viewed as particular cases of the memory function approach. Another advantage of this method is that it is highly flexible and customizable. We have shown here only the basic features, limiting ourselves to a simple memory function and to a scalar generalized Langevin equation, using the constant density \bar{n} as the only variable of interest. But, as mentioned previously, by using a vector composed of (1) the number density $n_{\mathbf{k}}(t)$, (2) the longitudinal current density $j_{\mathbf{k}}^L(t)$, and (3) the energy density $e_{\mathbf{k}}(t)$, we can build a matrix GLE containing a 3×3 memory matrix [49,50]. Following the same scheme as presented here, we can obtain the expression of a dielectric function that has embedded (i) the conservation of the number of particles, (ii) the conservation of the momentum, (iii) the conservation of the energy, and (iv) pair correlations. Moreover, we believe

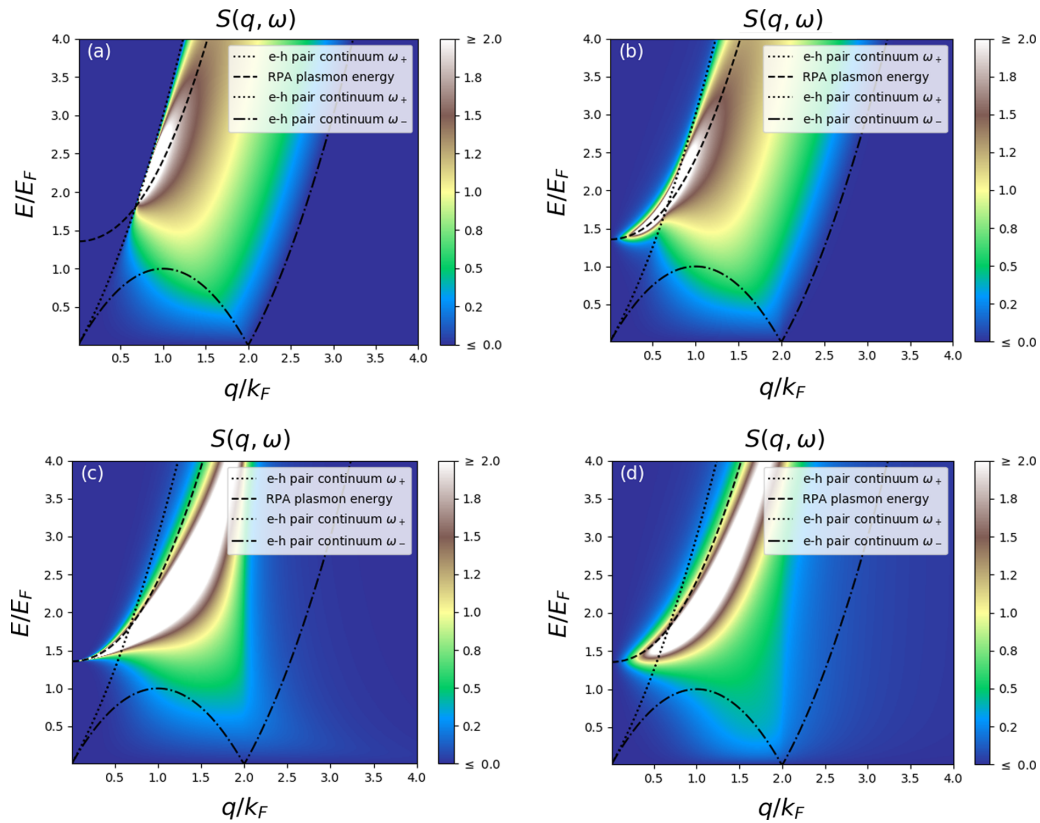


FIG. 9. Dynamic structure factors $S(\mathbf{q}, \omega)$ of aluminum for (a) RPA, (b) Mermin, (c) Nevanlinna (STA3), and (d) memory function (COCO) methods. We see clearly here that damping outside the Landau region is necessary to visualize the plasmon.

that the Atwal-Ashcroft approach [19] will be found to be a particular case of the 3×3 memory matrix method, as the Mermin method is a particular case of the memory function method.

If need be, this method can be further augmented by building on 4 moments, as it is known that $\langle \omega^5 \rangle$ incorporates three-body correlations [21]. The exact value of this term is very complicated, but reasonable approximations exist that allow one to compute it. Work is in progress to incorporate it into the MsSpec-DFM computer code.

The memory function approach we have used here relies on a single memory function, which means that it includes the relaxation of the system on a single timescale. In classical systems, such as the relaxation of a fluid, molecular dynamics seems to favor two-relaxation-time laws [57]. The memory matrix method we have outlined in the previous paragraph makes use of several memory functions. But even in the simpler method discussed here, we can accommodate several relaxation processes operating on different timescales, which in our case would describe different decay channels of the plasmon. This is the so-called mode-coupling framework [51–53] developed by Götze.

VII. CONCLUSION

In this work, we have tested different electron gas dielectric functions in order to ultimately model fluctuation potentials. These fluctuation potentials are the key quantity

in the multiple scattering description of plasmon features in spectroscopies such as photoemission or EELS.

We have presented three families of dielectric functions, RPA-based, damped RPA-based, and 3-moment reconstructed. We have shown that the simple RPA-based ones are not suited to our needs. Furthermore, as the damped type of dielectric functions can be shown to be a particular case of Götze’s memory function scheme, we have come to the conclusion that the memory function approach, to which the Nevanlinna one is strongly related, has all the features needed for a precise and accurate modeling. In addition, it can be improved by passing to the matrix approach and by incorporating the different plasmon decay channels and their timescale through the mode-coupling framework.

This approach is still based on the homogeneous electron gas model. Therefore, no band structure and no crystal structure is involved. We are currently investigating the influence of the band structure by performing *ab initio* calculations of $\varepsilon(\mathbf{q}, \omega)$ with the Questaal code [17,18]. This will allow us to benchmark our code and assess its limits when dealing with materials with complex band structures. Preliminary results point toward a minor influence, at least in the case of aluminum which has a simple band structure. Another line of research which we are currently pursuing in order to further improve our description is to couple this electron dielectric function to a phonon dielectric function. We are hopeful that all of these improvements will lead to a fast, efficient, and flexible approach to the modeling

of the dielectric function necessary to incorporate plasmon features into the multiple scattering description of spectroscopies.

The MsSpec-DFM code, built during this work, will be published soon as a separate module of the MsSpec code [12,13]. In addition to 3D dielectric functions, as exposed here, it will also contain the modeling of

other dimensionality, including graphene-type and multilayer structures.

ACKNOWLEDGMENT

A.M. is indebted to Rennes Métropole for providing her with two 6-month grants as a visiting scientist.

-
- [1] C. Biswas, A. K. Shukla, S. Banik, V. K. Ahire, and S. R. Barman, *Phys. Rev. B* **67**, 165416 (2003).
- [2] S. R. Barman (private communication).
- [3] J. Osterwalder, T. Greber, S. Hüfner, and L. Schlapbach, *Phys. Rev. B* **41**, 12495 (1990).
- [4] V. M. da Silva Santana, D. David, J. S. de Almeida, and C. Godet, *Braz. J. Phys.* **48**, 215 (2018).
- [5] C. Godet, D. David, V. M. da Silva Santana, J. S. de Almeida, and D. Sébilleau, in *Recent Advances in Thin Films* (Springer, Singapore, 2020), pp. 181–210.
- [6] M. Guzzo, G. Lani, F. Sottile, P. Romaniello, M. Gatti, J. J. Kas, J. J. Rehr, M. G. Silly, F. Sirotti, and L. Reining, *Phys. Rev. Lett.* **107**, 166401 (2011).
- [7] M. Guzzo, J. J. Kas, F. Sottile, M. G. Silly, F. Sirotti, J. J. Rehr, and L. Reining, *Eur. Phys. J. B* **85**, 324 (2012).
- [8] D. Vigil-Fowler, S. G. Louie, and J. Lischner, *Phys. Rev. B* **93**, 235446 (2016).
- [9] T. Fujikawa and H. Arai, *J. Electron Spectrosc. Relat. Phenom.* **123**, 19 (2002).
- [10] T. Fujikawa and H. Arai, *J. Electron Spectrosc. Relat. Phenom.* **149**, 61 (2005).
- [11] M. Kazama, H. Shinotsuka, Y. Otori, K. Niki, T. Fujikawa, and L. Kövér, *Phys. Rev. B* **89**, 045110 (2014).
- [12] D. Sébilleau, C. Natoli, G. M. Gavaza, H. Zhao, F. Da Pieve, and K. Hatada, *Comput. Phys. Commun.* **182**, 2567 (2011).
- [13] See <https://msspec.cnrs.fr>.
- [14] J. Inglesfield, *J. Phys. C* **16**, 403 (1983).
- [15] L. Hedin, J. Michiels, and J. Inglesfield, *Phys. Rev. B* **58**, 15565 (1998).
- [16] F. Bechstedt, R. Enderlein, and D. Reichardt, *Phys. Status Solidi (b)* **117**, 261 (1983).
- [17] See <http://www.questaal.org>.
- [18] J. Jackson, L. Petit, A. Mandal, and D. Sébilleau (unpublished).
- [19] G. S. Atwal and N. W. Ashcroft, *Phys. Rev. B* **65**, 115109 (2002).
- [20] K. Pathak and P. Vashishta, *Phys. Rev. B* **7**, 3649 (1973).
- [21] H. De Raedt and B. De Raedt, *Phys. Rev. B* **18**, 2039 (1978).
- [22] J. Koringa, *Physica* **13**, 392 (1947).
- [23] W. Kohn and N. Rostoker, *Phys. Rev.* **94**, 1111 (1954).
- [24] W. Bardyszewski and L. Hedin, *Phys. Scr.* **32**, 439 (1985).
- [25] L. Hedin, *J. Phys.: Condens. Matter* **11**, R489 (1999).
- [26] E. Wikborg and J. Inglesfield, *Phys. Scr.* **15**, 37 (1977).
- [27] W. Götze and P. Wölfle, *Phys. Rev. B* **6**, 1226 (1972).
- [28] W. G. Aulbur, L. Jönsson, and J. W. Wilkins, *Solid State Phys.* **54**, 1 (2000).
- [29] J. Lindhard, K. Dan. Vidensk. Selsk., Mat.-Fys. Medd. **28**, 8 (1954).
- [30] K. Utsumi and S. Ichimaru, *Phys. Rev. B* **22**, 1522 (1980).
- [31] A. Kugler, *J. Stat. Phys.* **12**, 35 (1975).
- [32] N. D. Mermin, *Phys. Rev. B* **1**, 2362 (1970).
- [33] H. B. Nersisyan and A. K. Das, *Phys. Rev. E* **69**, 046404 (2004).
- [34] G. Y. Hu and R. F. O’Connell, *Phys. Rev. B* **40**, 3600 (1989).
- [35] Y. V. Arkhipov, A. Askaruly, D. Ballester, A. E. Davletov, G. M. Meirkanova, and I. M. Tkachenko, *Phys. Rev. E* **76**, 026403 (2007).
- [36] V. Jindal, H. Singh, and K. Pathak, *Phys. Rev. B* **15**, 252 (1977).
- [37] D. Pines, *Elementary Excitations in Solids* (CRC Press, 2018).
- [38] Y. V. Arkhipov, A. Ashikbayeva, A. Askaruly, A. Davletov, and I. Tkachenko, *Europhys. Lett.* **104**, 35003 (2013).
- [39] I. Tkachenko, *Phys. Sci. Technol.* **5**, 16 (2018).
- [40] D. Y. Dubovtsev, Ph.D. thesis, Universidad Politécnic de Valencia, 2019, <http://hdl.handle.net/10251/125711>.
- [41] Y. V. Arkhipov, A. Ashikbayeva, A. Askaruly, A. Davletov, and I. Tkachenko, *Contrib. Plasma Phys.* **53**, 375 (2013).
- [42] Y. V. Arkhipov, A. B. Ashikbayeva, A. Askaruly, A. E. Davletov, and I. M. Tkachenko, *Phys. Rev. E* **90**, 053102 (2014).
- [43] S. Adamjan, T. Meyer, and I. Tkachenko, *Contrib. Plasma Phys.* **29**, 373 (1989).
- [44] F. Yoshida and S. Takeno, *Phys. Rep.* **173**, 301 (1989).
- [45] H. H. L. Umberto Balucani and V. Tognetti, *Phys. Rep.* **373**, 409 (2003).
- [46] K. Kumari and N. Singh, *Eur. J. Phys.* **41**, 053001 (2020).
- [47] R. Zwanzig, *Phys. Rev.* **124**, 983 (1961).
- [48] H. Mori, *Prog. Theor. Phys.* **33**, 423 (1965).
- [49] R. D. Mountain, *Adv. Mol. Relax. Processes* **9**, 225 (1976).
- [50] J.-P. Hansen and I. R. McDonald, *Theory of Simple Liquids* (Academic Press, 2005).
- [51] D. R. Reichman and P. Charbonneau, *J. Stat. Mech.* (2005) P05013.
- [52] L. M. C. Janssen, *Front. Phys.* **6**, 97 (2018).
- [53] W. Götze and L. Sjögren, *Transp. Theory Stat. Phys.* **24**, 801 (1995).
- [54] A. A. Khamzin, R. Nigmatullin, and I. I. Popov, *Theor. Math. Phys.* **173**, 1604 (2012).
- [55] C. Lemell, S. Neppel, G. Wachter, K. Tórkési, R. Ernstorfer, P. Feulner, R. Kienberger, and J. Burgdörfer, *Phys. Rev. B* **91**, 241101(R) (2015).
- [56] W. Götze, *Solid State Commun.* **27**, 1393 (1978).
- [57] I. Snook, *The Langevin and Generalised Langevin Approach to the Dynamics of Atomic, Polymeric and Colloidal Systems* (Elsevier, 2006).